This is the peer-reviewed, final accepted version for American Mineralogist, published by the Mineralogical Society of America.
The published version is subject to change. Cite as Authors (Year) Title. American Mineralogist, in press.
DOI: https://doi.org/10.2138/am-2022-7994. http://www.minsocam.org/

Revision 1

Nitscheite, $(NH_4)_2[(UO_2)_2(SO_4)_3(H_2O)_2]\cdot 3H_2O$, a new mineral with an unusual uranyl-sulfate sheet

ANTHONY R. KAMPF[1§], TRAVIS A. OLDS[2], JAKUB PLÁŠIL[3], BARBARA P. NASH[4], AND JOE MARTY[5]

[1] Mineral Sciences Department, Natural History Museum of Los Angeles County, 900 Exposition Boulevard, Los Angeles, CA 90007, USA
[2] Section of Minerals and Earth Sciences, Carnegie Museum of Natural History, 4400 Forbes Avenue, Pittsburgh, Pennsylvania 15213, USA
[3] Institute of Physics ASCR, v.v.i., Na Slovance 1999/2, 18221 Prague 8, Czech Republic
[4] Department of Geology and Geophysics, University of Utah, Salt Lake City, Utah 84112, USA
[5] 5199 East Silver Oak Road, Salt Lake City, UT 84108, USA

ABSTRACT

Nitscheite (IMA2020-078), $(NH_4)_2[(UO_2)_2(SO_4)_3(H_2O)_2]\cdot 3H_2O$, is a new mineral species from the Green Lizard mine, Red Canyon, San Juan County, Utah, U.S.A. It is a secondary phase found in association with chinleite-(Y), gypsum, pyrite, and Co-rich rietveldite. Nitscheite occurs in subparallel and divergent intergrowths of yellow prisms, up to about 0.3 mm in length. Crystals are elongated on [101] and exhibit the forms {100}, {010}, {001}, and {11-1}. The mineral is transparent with vitreous luster and very pale-yellow streak. It exhibits bright green

§ Email: akampf@nhm.org

fluorescence under a 405 nm laser. The Mohs hardness is ~2. The mineral has brittle tenacity, curved fracture, and one good cleavage on {010}. The measured density is 3.30(2) g·cm^{-3}. The mineral is easily soluble in RT H_2O. The mineral is optically biaxial (–), α = 1.560(2), β = 1.582(2), γ = 1.583(2) (white light); $2V_{meas}$ = 17(1)°; no dispersion; orientation X = **b,** $Z \approx$ [101]; pleochroism X colourless, Y and Z yellow; $X < Y \approx Z$. Electron microprobe analysis provided the empirical formula $(NH_4)_{1.99}U_{2.00}S_{3.00}O_{21}H_{10.01}$. Nitscheite is monoclinic, $P2_1/n$, a = 17.3982(4), b = 12.8552(3), c = 17.4054(12) Å, β = 96.649(7)°, V = 3866.7(3) Å^3, and Z = 8. The structure (R_1 = 0.0329 for 4547 $I > 3\sigma I$ reflections) contains $[(UO_2)_2(SO_4)_3(H_2O)_2]^{2-}$ uranyl-sulfate sheets, which are unique among minerals, with NH_4 and H_2O groups between the sheets.

Keywords: nitscheite; new mineral; uranyl sulfate sheet; crystal structure; Raman spectroscopy; Green Lizard mine, Red Canyon, Utah.

INTRODUCTION

Inactive uranium mines have proven to be fruitful underground "natural laboratories". Since 2012, the abandoned uranium mines in Red Canyon in southeastern Utah have provided more than 30 new uranyl minerals, predominantly uranyl sulfates, some of which possess bizarre structural features that have not been observed in laboratory synthetic experiments. The great diversity observed for uranyl sulfate minerals stems primarily from the large number of stable combinatorial linkages of uranyl pentagonal bipyramids and sulfate tetrahedra. The recent discoveries of novel structural topologies provide insight into the factors driving the crystallization of uranium minerals, in particular the relationship between mineral associations, local chemistry, and resulting structural topology. The formation of these mineral structures is strongly affected by at least three parameters: pH, cation content, and water content (Plášil et al. 2014). However, despite our growing knowledge of the crystal chemistry of uranyl sulfates, the cause of certain structural phenomena, manifested in particular in the minerals from Red Canyon, remains unknown. For instance, finite cluster topologies are relatively abundant among the sodium-uranyl-sulfate minerals, which occur commonly at the Blue Lizard mine, but do not occur in other mines nearby. Each new mineral has filled gaps in our understanding of how formation conditions influence the observed structural topologies, which is key to understanding the crystal-chemical nature of U-S systems, as well as to the entirety of uranyl mineralogy. The new uranyl sulfate nitscheite, described herein, possesses a type of uranyl sulfate sheet not previously observed in Nature.

Nitscheite is named in honor of German/American nuclear chemist Heino Nitsche (1949-2014) for his work on nuclear and radiochemistry of heavy elements, nuclear forensics, the chemistry of irradiated materials, and the confirmation of elements 114 (flerovium, Fl) and 117 (Tennessine, Ts). Most recently, Nitsche was full professor in the Department of Chemistry at the University of California, Berkeley, a senior research scientist at Lawrence Berkeley National Laboratory (LBNL), and the founding director of LBNL's Glenn T. Seaborg Center. In 2014, Nitsche won the Hevesy Medal, the premier international award of excellence honoring outstanding achievements in radioanalytical and nuclear chemistry.

Although the K analogue of nitscheite has been synthesized (Kornyakov et al. 2020), we do not propose the use of a -(NH_4) suffix in the naming of nitscheite at this time because no K was detected in its composition. If the K analogue is found to occur naturally, we recommend that nitscheite be used as the rootname for both species with -(NH_4) and -(K) suffixes added to distinguish them.

The new mineral and name were approved by the Commission on New Minerals, Nomenclature and Classification of the International Mineralogical Association (IMA 2020-078). The holotype specimen of nitscheite is deposited in the collections of the Natural History Museum of Los Angeles County, Los Angeles, California, USA, catalogue number 74163.

Occurrence

Nitscheite was found on specimens collected underground in the Green Lizard mine (37°34'37.10"N 110°17'52.80"W), Red Canyon, White Canyon District, San Juan County, Utah, USA. The mine is about 72 km west of the town of Blanding, Utah, and about 22 km southeast of Good Hope Bay on Lake Powell. It is located near the head of Low Canyon on the east side of Red Canyon, 2.1 km north of the Blue Lizard mine. The geology of the mine is similar to that of the Blue Lizard mine (Kampf et al. 2017b; Chenoweth 1993). The Green Lizard mine is also a type locality for shumwayite (Kampf et al. 2017a), greenlizardite (Kampf et al. 2018a), meitnerite (Kampf et al. 2018b), and straßmannite (Kampf et al. 2019).

Abundant secondary uranium mineralization in Red Canyon is associated with post-mining oxidation of asphaltum-rich sandstone beds laced with uraninite and sulfides in the damp underground environment. Nitscheite is a very rare mineral in the secondary mineral assemblages of the Green Lizard mine. It occurs with chinleite-(Y), gypsum, pyrite, and Co-rich rietveldite on matrix comprised mostly of subhedral to euhedral, equant quartz crystals that are recrystallized counterparts of the original grains of the sandstone.

Physical and Optical Properties

Nitscheite occurs in subparallel and divergent intergrowths of yellow prisms, up to about 0.3 mm in length (Fig. 1). Crystals are elongated on [101] and exhibit the forms {100}, {010}, {001}, and {11-1} (Fig. 2). [001/0-10/100] twinning by metric merohedry was identified based on the analysis of structure data. The mineral is transparent with vitreous luster and very pale-yellow streak. It exhibits bright green fluorescence under a 405 nm laser. It has a Mohs hardness of about 2 based on scratch tests. The mineral has brittle tenacity, curved fracture, and one good cleavage on {010}. The density measured by flotation in a mixture of methylene iodide and toluene is 3.30(2) g·cm^{-3}. The density calculated using the empirical formula and single-crystal unit cell parameters is 3.278 g·cm^{-3}. The mineral is easily soluble in H_2O at room temperature.

Nitscheite is optically biaxial (–) with α = 1.560(2), β = 1.582(2), γ = 1.583(2) measured in white light). The 2*V* measured using extinction data analyzed with EXCALIBRW (Gunter et al. 2004) is 17(1)°; the calculated 2*V* is 23.8°. No dispersion was observed. The optical orientation is *X* = **b,** *Z* ≈ [101]. The mineral is pleochroic with *X* colorless, *Y* and *Z* yellow; *X* < *Y* ≈ *Z*. The Gladstone–Dale compatibility, 1 – (K_P/K_C), (Mandarino 2007) is -0.010 (superior) based on the empirical formula using *k*(UO_3) = 0.118, as provided by Mandarino (1976).

RAMAN SPECTROSCOPY

Raman spectroscopy was conducted on a Horiba XploRA PLUS using a 100× (0.9 NA) objective. The spectrum from 4000 to 60 cm^{-1} obtained using a 532 nm diode laser, 50 μm slit, and 2400 gr/mm diffraction grating is shown in Figure 3. The spectrum from 2000 to 60 cm^{-1} obtained using a 785 nm diode laser, 50 μm slit, and 1800 gr/mm diffraction grating is shown in Figure 4. The band assignments are based primarily upon those for uranyl sulfate minerals provided by Čejka (1999) and Plášil et al. (2010). All bands in the spectra were fit using pseudo-Voigt peak profiles.

A multitude of weak bands between ~2800 and 3600 cm^{-1} in the spectrum obtained using the 532 nm laser are assigned to ν (OH) and ν (NH) stretching vibrations of interlayer NH_4^+ groups. Using the empirically derived equation of Libowitzky (1999), the calculated distances of the corresponding hydrogen bonds range from ~3.3 Å to ~2.6 Å, in reasonable agreement with the O···O/N bond lengths determined from the structure refinement. Several very broad low intensity bands between ~2200 and ~1800 cm^{-1} are probably overtones or combination bands. In both 532 and 785 nm spectra, no apparent band related to the ν_2 (δ) bending vibrations of H_2O is present at approximately 1600 cm^{-1}, which is not surprising considering the low sensitivity of Raman for the non-symmetrical vibrations. Due to the strong fluorescence observed with 532 nm laser illumination, we continue our discussion of band assignments using fittings obtained from the 785 nm spectrum.

The ν_3 (SO_4) antisymmetric stretching vibrations occur as weak bands at 1202, 1156, 1134, and 1102 cm^{-1}. Several weak to strong bands at 1047, 1038, 1030, 1020, 1007, 993, and 977 cm^{-1} are assignable to the ν_1 symmetric stretching vibration of SO_4 groups. The presence of six symmetrically distinct SO_4 tetrahedra in the structure of nitscheite leads to the multiple split bands in this region. The ν_1 $(UO_2)^{2+}$ symmetric stretching vibration is present as a very strong band at 856 cm^{-1}, with a weaker, overlapping shoulder at 852 cm^{-1}. Bartlett and Cooney (1989) provided an empirical relationship to derive the approximate U–O_{Ur} bond lengths from the band position assigned to the UO_2^{2+} stretching vibrations, which gives 1.75 Å (856 cm^{-1}) and 1.76 Å (852 cm^{-1}), in excellent agreement with the average U1–O_{Ur} bond length from the X-ray data: 1.763 Å. At least five overlapping weak bands between ~650 and 600 cm^{-1} are attributable to the ν_4 (δ) (SO_4) bending vibrations, with centers at 650, 639, 629, 620, and 614 cm^{-1}. Weak bands at 457, 451, and 443 cm^{-1} belong to the ν_2 (δ) (SO_4) bending vibrations. A set of very broad and very weak bands between ~400 and 350 cm^{-1} likely are due to out-of-plane bending vibrations of U–O_{eq} bonds in the sheet. A complex group of bands between 250 cm^{-1} and ~220 cm^{-1}, with centers at 279, 265, 260, 255, and 228 cm^{-1} are attributable to the doubly degenerate ν_2 (δ) $(UO_2)^{2+}$ bending vibrations and possibly to ν (U–O_{eq}) bending modes. The remaining bands below ~200 cm^{-1} arise due to unassigned phonon modes and molecular deformations.

Chemical Analysis

Electron probe microanalyses (5 points on 5 crystals) were performed at the University of Utah on a Cameca SX-50 electron microprobe with four wavelength dispersive spectrometers and using Probe for EPMA software. Analytical conditions were 15 kV accelerating voltage, 10 nA beam current, and 10 μm beam diameter. Raw X-ray intensities were corrected for matrix effects with a ϕρ(z) algorithm (Pouchou and Pichoir 1991). Because of the presence of substantial H_2O, the formula concentration of oxygen was used in the matrix correction. A synthetic PC1 W/Si multilayer "crystal" was used for N analysis. Time-dependent, log-linear, corrections were applied to N (decreasing intensity) and U (increasing intensity). No other elements were detected. There was major beam damage. Because insufficient material is available for a direct determination of H_2O, it has been calculated based upon the structure (U = 2 *apfu* and O = 21 *apfu*). Analytical data are given in Table 1. The empirical formula is $(NH_4)_{1.99}U_{2.00}S_{3.00}O_{21}H_{10.00}$. The ideal formula is $(NH_4)_2[(UO_2)_2(SO_4)_3(H_2O)_2]\cdot 3H_2O$, which requires $(NH_4)_2O$ 5.46, UO_3 59.94, SO_3 25.17, H_2O 9.44, total 100 wt%.

X-ray crystallography and structure determination

Both powder and single-crystal X-ray studies were carried out using a Rigaku R-AXIS Rapid II curved imaging plate microdiffractometer with monochromatized Mo*K*α radiation. For the powder study, a Gandolfi-like motion on the φ and ω axes was used to randomize the sample, which consisted of several crystals. Observed *d* values and intensities were derived by profile fitting using JADE 2010 software (Materials Data, Inc. Livermore, CA). The observed powder diffraction pattern compares very well with the pattern calculated from the crystal structure; data are given in Supplemental[1] Table S1.

Crystals occur in subparallel intergrowths making the selection of a single crystal challenging. The crystal fragment used for the data collection comprised one major crystal and several subparallel satellite crystals. Initial indexing of single-crystal reflections suggested an orthorhombic unit cell: a = 11.5685(3), b = 12.8520(9), c = 12.9949(4) Å. This is comparable to the cells reported for synthetic $(NH_4)_2(UO_2)_2(SO_4)_3 \cdot 5H_2O$ (Staritzky et al. 1956) and analogous phases such as $Rb_2(UO_2)_2(SO_4)_3 \cdot 5H_2O$ (Serezhkina et al. 1990), which were purported to be orthorhombic with likely space group *Pnma* based on PXRD data, but without structure determination. Furthermore, the PXRD of nitscheite is a close match to those for these synthetic phases. We were unable to solve the structure using this cell and any orthorhombic space group. Ultimately, we solved the structure in space group $P2_1/n$ using the larger (×2) monoclinic cell reported (Table 2). The metrically orthorhombic cell noted above is a subcell of our monoclinic cell (see Fig. 5). Recently, Kornyakov et al. (2020) reported the structure of the synthetic K analogue of nitscheite, α-$K_2[(UO_2)_2(SO_4)_3(H_2O)_2](H_2O)_3$, also with space group $P2_1/n$ and with a comparable monoclinic cell.

The structure data for nitscheite were processed using the Rigaku CrystalClear software package, including the application of an empirical multi-scan absorption correction using

DOI: https://doi.org/10.2138/am-2022-7994. http://www.minsocam.org/

ABSCOR (Higashi, 2001). The structure was solved using SHELXT (Sheldrick, 2015a). Refinement proceeded by full-matrix least-squares on F^2 using SHELXL-2016 (Sheldrick, 2015b). Most atoms were located in the initial structure solution and the remaining non-hydrogen atoms were located in subsequent difference Fourier syntheses. At this stage, only U and S sites could be successfully refined with anisotropic displacement parameters, R_1 (for 5006 $I > 2\sigma I$ reflections) converged to a high value: 0.093, there were high positive and negative electron residuals (+5.29 and –4.88 $e\cdot$Å^{-3}), and there were some anomalous interatomic distances. Kornyakov et al. (2020) reported similar issues with their refinement of the structure of α-$K_2[(UO_2)_2(SO_4)_3(H_2O)_2](H_2O)_3$, and related them to the twinning due to pseudo-merohedry. The HKLF5 type of reflection file created by the utility in PLATON (Spek 2003) was found as the only way to handle the twinning successfully. Twinning in nitscheite is by reticular merohedry; the mirror in {101}, expressed by the matrix | 0 0 -1 | 0 1 0 | -1 0 0 | causes twinning of the nitscheite cell, which gives arise to an orthorhombic supercell, with a = 12.855 Å, b = 23.141 Å, c = 25.996 Å, α = 89.98°, β = 90°, γ = 90°, and V = 2*3866.7 Å^3. The subsequent refinement in the JANA2006 program (Petříček et al. 2016), using the HKLF5 file and invoking the abovementioned twinning resolved all of the issues encountered in our initial structure refinement. All non-hydrogen atom sites were refined to full occupancies with anisotropic displacement parameters; however, difference Fourier syntheses were unsuccessful in locating hydrogen atom positions. The refined twin ratio equals to 0.7304(11)/0.2696(11). The refinement converged to R_1 = 3.29% for 4547 reflections with $I > 3\sigma(I)$. Data collection and refinement details are given in Table 2, atom coordinates and displacement parameters can be found in the original CIF (as supplemental file[1]), selected bond distances in Table 3, and a bond-valence analysis in Table 4.

DOI: https://doi.org/10.2138/am-2022-7994. http://www.minsocam.org/

DESCRIPTION OF THE STRUCTURE

Four U sites (U1, U2, U3, and U4) in the structure of nitscheite are each surrounded by seven O atoms forming squat UO_7 pentagonal bipyramids. This is a typical coordination for U^{6+} in which the two short apical bonds of the bipyramid constitute the uranyl group (Burns, 2005). The two apical O atoms of the bipyramids (O_{Ur}) form short bonds with the U, and this unit comprises the UO_2^{2+} uranyl group. Five equatorial O atoms (O_{eq}) complete the U coordination environment, some of which include O of H_2O groups with long U–O bond distances >2.4 Å. The U1 site bonds with two H_2O groups (Ow3 and Ow4), U2 and U3 bond with a single H_2O group (Ow1 and Ow2, respectively), and U4 forms no bonds with H_2O groups.

There are six S sites (S1, S2, S3, S4, S5, and S6) each centering an SO_4 tetrahedron. The SO_4 tetrahedra share corners with the equatorial O atoms of the UO_7 bipyramids to form a uranyl-sulfate sheet with the composition $[(UO_2)_2(SO_4)_3(H_2O)_2]^{2-}$ (Fig. 5). Within this sheet, the U1 bipyramid shares three of its O_{eq} corners with SO_4 groups, the U2 and U3 bipyramids each share four of their O_{eq} corners with SO_4 groups, and the U4 bipyramid shares all five of its O_{eq} corners with SO_4 groups. The uranyl-sulfate sheet in the structure of nitscheite is unique in the mineral kingdom, but it has the same topology as the sheet in α-$K_2[(UO_2)_2(SO_4)_3(H_2O)_2](H_2O)_3$ and β-$K_2[(UO_2)_2(SO_4)_3(H_2O)_2](H_2O)_3$ (Kornyakov et al. 2020), and it has similarities to those in several minerals and other synthetic phases (See Table 5 and Figure 5 in Lussier et al. 2016).

The interlayer region between the uranyl sulfate sheets (Fig. 6) contains four NH_4 sites (N1, N2, N3, and N4) and six H_2O sites (OW5, OW6, OW7, OW8, OW9, and OW10). Each of the NH_4 sites is eight-coordinated (for N–O < 3.44 Å), linking to at least three O sites in the adjacent negatively charged sheets and providing essential charge balance.

This is the peer-reviewed, final accepted version for American Mineralogist, published by the Mineralogical Society of America.
The published version is subject to change. Cite as Authors (Year) Title. American Mineralogist, in press.
DOI: https://doi.org/10.2138/am-2022-7994. http://www.minsocam.org/

It is noteworthy that the structural complexity (after Krivovichev 2012, 2013, 2014, 2018) of nitscheite, $I_{G,total}$, is very high, 2400.67 bits/cell (including a theoretical positions of the H atoms). Nitscheite is the second most complex uranyl sulfate mineral known, following closely behind natrozippeite, with 2528.63 bits/cell (Gurzhiy and Plášil 2019). Both minerals have unit-cell volumes greater than 3500 Å^3 and their structures are characterized by very large numbers of hydrogen bonds.

IMPLICATIONS

Recent investigations of synthetic and natural alkali and alkaline earth uranyl sulfate hydrates have shown that these phases adopt highly diverse bonding arrangements based on cluster, chain, sheet, and framework topologies (Gurzhiy and Plášil 2019; Tyumentseva et al. 2019; Kornyakov et al. 2020). This is partly due to the large degree of freedom of polymerization between U and SO_4 groups, as well as significant variability in coordination geometry of Na, K, and NH_4 cations, permitting a large number of crystal-chemically stable structures to form with only minor differences in U:S:*Me*:H_2O content. Other factors such as pH and relative humidity influence the structure of these phases due to extensive variability in hydrogen bonding, while idiosyncrasies in associated minerals, along with sequential dissolution or crystallization on unique substrates has formed mineral structures that have not yet been reproduced under laboratory conditions.

For example, the mineral geschieberite, $K_2[(UO_2)(SO_4)_2(H_2O)](H_2O)$ (Plášil et al. 2015), which has a higher H_2O and S:U content than nitscheite, forms a distinct sheet topology due to the depolymerizing action of an equatorially bonded H_2O group about the U atom in its structure. Such is also the case for the mineral beshtauite, $(NH_4)_2(UO_2)(SO_4)_2(H_2O)_2$ (Pekov et al. 2014), which contains a topology closely related to that of geschieberite – the only difference being an alternating directionality of equatorial H_2O groups in their sheets. The cause of this subtle topological "flip" is unknown and, although NH_4^+ and K^+ cations commonly substitute to form isomorphic minerals, we note that the potential K-analogue of nitscheite may adopt a similarly unique topological arrangement (Fig. 7). Nitscheite contains U sites with 0, 1, and 2 equatorially bonded H_2O groups, arranged into the unique and novel topology described here.

It is unfortunate that the recent permanent sealing of all mines in Red Canyon and surrounding areas, enforced by the State of Utah and funded by the U.S. Department of Energy, has eliminated access to one of the most remarkable sources of uranyl sulfate minerals on Earth. The study of the diverse secondary mineralogy of Utah's abandoned mines, which now must rely on previously collected samples, continues to yield invaluable insights into the environmental behavior of U in ways that only Nature can provide.

ACKNOWLEDGEMENTS

Reviewers Sergey Krivovichev and Fernando Colombo are thanked for constructive comments, which improved the manuscript. We are grateful to retired miner Dan Shumway of Blanding, Utah, for advice and assistance in our collecting efforts in Red Canyon. Funding to JP was provided by the Czech Science Foundation (20-11949S). This study was also funded by the John Jago Trelawney Endowment to the Mineral Sciences Department of the Natural History Museum of Los Angeles County.

REFERENCES

Bartlett, J.R. and Cooney, R.P. (1989) On the determination of uranium-oxygen bond lengths in dioxouranium(VI) compounds by Raman spectroscopy. Journal of Molecular Structure, 193, 295–300.

Burns, P.C. (2005) U^{6+} minerals and inorganic compounds: Insights into an expanded structural hierarchy of crystal structures. The Canadian Mineralogist, 43, 1839–1894.

Čejka J. (1999) Infrared spectroscopy and thermal analysis of the uranyl minerals. Pp. 521–622. In P.C. Burns, and R.C. Ewing, Eds. Uranium: Mineralogy, geochemistry and the environment, 38, Mineralogical Society of America.

Chenoweth, W.L. (1993) The Geology and Production History of the Uranium Deposits in the White Canyon Mining District, San Juan County, Utah. Utah Geological Survey Miscellaneous Publication, 93–3.

Gagné, O.C., and Hawthorne, F.C (2015) Comprehensive derivation of bond-valence parameters for ion pairs involving oxygen. Acta Crystallographica, B71, 562–578.

García-Rodríguez, L., Rute-Pérez, Á., Piñero, J.R. and González-Silgo, C. (2000) Bond-valence parameters for ammonium-anion interactions. Acta Crystallographica, B56, 565–569.

Gunter, M.E., Bandli, B.R., Bloss, F.D., Evans, S.H., Su, S.C., and Weaver, R. (2004) Results from a McCrone spindle stage short course, a new version of EXCALIBR, and how to build a spindle stage. The Microscope, 52, 23–39.

Gurzhiy V.V. and Plášil J. (2019) Structural complexity of natural uranyl sulfates. Acta Crystallographica, B75, 39–48.

Higashi, T. (2001) ABSCOR. Rigaku Corporation, Tokyo.

Kampf, A.R., Plášil, J., Kasatkin, A.V., Marty, J. Čejka, J. and Lapčák, L. (2017a) Shumwayite, $[(UO_2)(SO_4)(H_2O)_2]_2 \cdot H_2O$, a new uranyl sulfate mineral from Red Canyon, San Juan County, Utah, USA. Mineralogical Magazine, 81, 273–285.

Kampf A.R., Plášil J., Kasatkin A.V., Marty J. and Čejka J. (2017b) Klaprothite, péligotite and ottohahnite, three new sodium uranyl sulfate minerals with bidentate UO_7–SO_4 linkages from the Blue Lizard mine, San Juan County, Utah, USA. Mineralogical Magazine, 81, 753–779.

Kampf, A.R., Plášil, J., Nash, B.P. and Marty, J. (2018a) Greenlizardite, $(NH_4)Na(UO_2)_2(SO_4)_2(OH)_2 \cdot 4H_2O$, a new mineral with phosphuranylite-type uranyl sulfate sheets from Red Canyon, San Juan County, Utah, USA. Mineralogical Magazine, 82, 401–411.

Kampf, A.R., Plášil, J., Nash, B.P. and Marty, J. (2018b) Meitnerite, $(NH_4)(UO_2)(SO_4)(OH) \cdot 2H_2O$, a new uranyl-sulfate mineral with a sheet structure. European Journal of Mineralogy, 30, 999–1006.

Kampf, A.R., Plášil, J., Kasatkin, A.V., Nash, B.P. and Marty, J. (2019) Magnesioleydetite and straßmannite, two new uranyl sulfate minerals with sheet structures from Red Canyon, Utah. Mineralogical Magazine, 83, 349–360.

Krivovichev, S.V. (2012) Topological complexity of crystal structures: quantitative approach. Acta Crystallographica, A68, 393–398.

Krivovichev, S.V. (2013) Structural complexity of minerals: information storage and processing in the mineral world. Mineralogical Magazine, 77, 275–326.

Krivovichev, S.V. (2014) Which inorganic structures are the most complex? Angewandte Chemie, International Edition English, 53, 654–661.

Krivovichev, S.V. (2018) Ladders of information: what contributes to the structural complexity of inorganic crystals. Zeitschrift für Kristallographie, 233, 155–161.

Kornyakov, I.V., Tyumentseva, O.S., Krivovichev, S.V. and Gurzhiy, V.V. (2020) Dimensional evolution in hydrated K^+-bearing uranyl sulfates: from 2D-sheets to 3D-frameworks. CrystEngComm, 22, 4621–4629.

Libowitzky, E. (1999) Correlation of O-H stretching frequencies and O-H…O hydrogen bond lengths in minerals. Monatshefte für Chemie, 130, 1047–1059.

Lussier, A.J., Lopez, R.A. and Burns, P.C. (2016) A revised and expanded structure hierarchy of natural and synthetic hexavalent uranium compounds. The Canadian Mineralogist, 54, 177–283.

Mandarino, J.A. (1976) The Gladstone-Dale relationship – Part 1: derivation of new constants. Canadian Mineralogist, 14, 498–502.

Mandarino, J.A. (2007) The Gladstone–Dale compatibility of minerals and its use in selecting mineral species for further study. Canadian Mineralogist, 45, 1307–1324.

Pekov, I.V., Krivovichev, S.V., Yapaskurt, V.O., Chukanov, N.V. and Belakovskyi, D.I. (2014) Beshtauite, $(NH_4)_2(UO_2)(SO_4)2\cdot 2H_2O$, a new mineral from Mount Beshtau, Northern Caucasus, Russia. American Mineralogist, 99, 1783–1787.

Petříček, V., Dušek, M. and Plášil, J. (2016) Crystallographic computing system Jana2006: Solution and refinement of twinned structures. Zeitschrift für Kristallographie, 231, 583–599.

Plášil, J., Buixaderas, E., Čejka, J., Sejkora, J., Jehlička, J. and Novák, M. (2010) Raman spectroscopic study of the uranyl sulphate mineral zippeite: low wavenumber and U-O stretching regions. Analytical and Bioanalytical Chemistry, 397, 2703–2715.

Plášil, J., Hloušek, J., Kasatkin, A.V., Škoda, R., Novák, M. and Čejka, J. (2015) Geschieberite, $K_2(UO_2)(SO_4)_2(H_2O)_2$, a new uranyl sulfate mineral from Jáchymov. Mineralogical Magazine, 79, 205–216.

Pouchou, J.-L. and Pichoir, F. (1991) Quantitative Analysis of Homogeneous or Stratified Microvolumes Applying the Model "PAP." Pp. 31–75 in: Electron Probe Quantitation. Springer US, Boston, MA.

Serezhkina, L., Shirinova, A. and Serezhkin, V. (1990) Complex formation in the system Rb_2SO_4-UO_2SO_4-H_2O at 25°C. Journal of Inorganic Chemistry, 35, 260.

Sheldrick, G.M. (2015a) SHELXT - Integrated space-group and crystal-structure determination. Acta Crystallographica, A71, 3–8.

Sheldrick, G.M. (2015b) Crystal Structure refinement with SHELX. Acta Crystallographica, C71, 3–8.

Spek, A.L. (2003) Single-crystal structure validation with the program PLATON. Journal of Applied Crystallography, 36, 7–13.

Staritzky, E., Cromer, D.T. and Walker, D.I. (1956) Diammonium diuranyl trisulfate pentahydrate, $(NH_4)_2(UO_2)_2(SO_4)_3{\cdot}5H_2O$. Analytical Chemistry, 28, 1634-1635.

Tyumentseva, S.O., Kornyakov, V.I., Britvin, N.S., Zolotarev, A.A. and Gurzhiy V.V. (2019) Crystallographic insights into uranyl sulfate minerals formation: Synthesis and crystal structures of three novel cesium uranyl sulfates. Crystals, 9, 660.

Endnote:

[1]Deposit item AM-21-XXXXX, Supplemental tables and CIF. Deposit items are free to all readers and found on the MSA website, via the specific issue's Table of Contents (go to http://www.minsocam.org/MSA/AmMin/TOC/2021/Xxx2021_data/ Xxx2021_data.html).

FIGURE CAPTIONS

Figure 1. Nitscheite prisms with gypsum and pyrite on quartz. The field of view is 0.5 mm across.

Figure 2. Crystal drawing of nitscheite (clinographic projection in non-standard orientation, [101] vertical).

Figure 3. The Raman spectrum of nitscheite recorded with a 532 nm laser.

Figure 4. The fitted baseline-corrected Raman spectrum of nitscheite recorded with a 785 nm laser.

Figure 5. The $[(UO_2)_2(SO_4)_3(H_2O)_2]$ sheet in nitscheite viewed down [010]. UO_7 and SO_4 polyhedra are labelled. The unit cell outline is indicated by dashed black lines. The outline of the metrically orthorhombic subcell is shown by dashed red lines with cell edge lengths labeled. (color online).

Figure 6. The crystal structure of nitscheite viewed down [001]. N atoms of NH_4 groups are small red balls and O atoms of interlayer H_2O groups are large white balls. The unit cell is indicated by dashed lines. (color online)

Figure 7. Cation topology of (a) nitscheite and (b) synthetic α-$K_2[(UO_2)_2(SO_4)_3(H_2O)_2](H_2O)_3$ (Kornyakov et al. 2020). Interlayer cations (large balls: N-blue, K-magenta) are projected on U-S layers (small balls: U-yellow, S-blue). (color online)

Table 1. Chemical composition of nitscheite.

Constituent	**Mean**	**Range**	**Stand. Dev.**	**Standard**
$(NH_4)_2O$	5.42	4.18–6.32	0.89	syn. Cr_2N
UO_3	59.75	57.33–62.09	1.70	syn. UO_2
SO_3	25.12	24.34–25.76	0.72	celestine
H_2O*	9.41			
Total	**99.70**			

* based upon the structure (U = 2 *apfu* and O = 21 *apfu*).

Table 2. Data collection and structure refinement details for nitscheite.

Diffractometer	Rigaku R-Axis Rapid II
X-ray radiation/power	Mo*K*α (λ = 0.71075 Å)/50 kV, 40 mA
Temperature	293(2) K
Structural Formula	$(NH_4)_2[(UO_2)_2(SO_4)_3(H_2O)_2]\cdot3H_2O$ (H atoms not located)
Space group	$P2_1/n$
Unit cell dimensions	*a* = 17.3982(4) Å
	b = 12.8552(3) Å
	c = 17.4054(12) Å
	β = 96.649(7)°
V	3866.7(3) $Å^3$
Z	8
Density (for above formula)	3.251 $g\cdot cm^{-3}$
Absorption coefficient	17.157 mm^{-1}
F(000)	3392
Crystal size	170 × 25 × 20 μm
θ range	3.13 to 25.04°
Index ranges	$-20 \le h \le 20$, $0 \le k \le 15$, $0 \le l \le 20$
Reflections collected/unique	35158/6491; R_{int} = 0.081
Reflections with $I > 3\sigma I$	4547
Completeness to θ = 25.04°	95.2%
Refinement method	Full-matrix least-squares on F^2
Parameters/restraints	506/0
GoF	1.181
Refined twin ratio	0.7304(11)/0.2696(11)
Final *R* indices [$F > 4\sigma(F)$]	R_1 = 0.0329, wR_2 = 0.0681
R indices (all data)	R_1 = 0.0532, wR_2 = 0.0752
Weighting scheme, weights	Weighting scheme based on measured s.u.'s; $w = 1/(\sigma^2(I) + 0.0004I^2)$
Largest diff. peak/hole	+2.58/–1.32 $e\cdot Å^{-3}$

Table 3. Selected bond distances (Å) for nitscheite.

N1–O17	2.803(15)	N2–O9	2.775(16)	N3–O13	2.976(18)	N4–O8	2.946(14)
N1–O18	2.884(15)	N2–O10	2.817(16)	N3–OW10	2.98(2)	N4–O21	2.987(17)
N1–O5	2.935(15)	N2–O13	2.980(16)	N3–O3	2.991(16)	N4–O23	2.995(14)
N1–O21	3.018(15)	N2–O1	3.005(16)	N3–O16	3.014(16)	N4–O5	3.003(18)
N1–O30	3.042(16)	N2–O26	3.051(17)	N3–OW6	3.03(2)	N4–OW5	3.06(2)
N1–OW8	3.171(18)	N2–OW7	3.101(18)	N3–O1	3.044(17)	N4–OW9	3.06(2)
N1–O27	3.279(16)	N2–O28	3.320(17)	N3–O2	3.072(15)	N4–O24	3.076(15)
N1–O25	3.305(16)	N2–O31	3.324(17)	N3–O14	3.173(16)	N4–O7	3.232(15)
<N1–O>	3.055	<N2–O>	3.047	<N3–O>	3.035	<N4–O>	3.045
U1–O25	1.765(9)	U2–O27	1.751(10)	U3–O29	1.746(10)	U4–O31	1.750(10)
U1–O26	1.766(10)	U2–O28	1.755(9)	U3–O30	1.762(9)	U4–O32	1.771(9)
U1–O4	2.323(7)	U2–O6	2.335(11)	U3–O19	2.364(9)	U4–O15	2.337(8)
U1–O23	2.333(9)	U2–O12	2.367(7)	U3–O16	2.371(8)	U4–O8	2.374(7)
U1–O24	2.378(8)	U2–O3	2.372(8)	U3–O14	2.373(9)	U4–O11	2.375(9)
U1–OW4	2.423(9)	U2–O2	2.381(9)	U3–O22	2.377(9)	U4–O7	2.393(9)
U1–OW3	2.446(9)	U2–OW1	2.495(9)	U3–OW2	2.429(8)	U4–O20	2.398(8)
<U1–O_{ap}>	1.766	<U2–O_{ap}>	1.753	<U3–O_{ap}>	1.754	<U4–O_{ap}>	1.761
<U1–O_{eq}>	2.381	<U2–O_{eq}>	2.390	<U3–O_{eq}>	2.383	<U4–O_{eq}>	2.375
S1–O1	1.462(10)	S2–O5	1.414(11)	S3–O9	1.449(11)		
S1–O2	1.474(9)	S2–O6	1.471(11)	S3–O10	1.456(9)		
S1–O3	1.483(9)	S2–O7	1.479(10)	S3–O11	1.482(10)		
S1–O4	1.488(8)	S2–O8	1.490(8)	S3–O12	1.501(8)		
<S1–O>	1.477	<S2–O>	1.464	<S3–O>	1.472		
S4–O13	1.442(11)	S5–O17	1.438(11)	S6–O21	1.436(11)		
S4–O15	1.474(10)	S5–O18	1.465(10)	S6–O22	1.466(9)		
S4–O16	1.479(9)	S5–O19	1.496(9)	S6–O23	1.498(10)		
S4–O14	1.480(10)	S5–O20	1.507(10)	S6–O24	1.507(9)		
<S4–O>	1.469	<S5–O>	1.477	<S6–O>	1.477		

Table 4. Bond valence analysis for nitscheite. Values are expressed in valence units.*

	N1	N2	N3	N4	U1	U2	U3	U4	S1	S2	S3	S4	S5	S6	sum
O1		0.12	0.11						1.54						1.77
O2			0.10			0.49			1.49						2.08
O3			0.13			0.50			1.46						2.09
O4					0.56				1.44						2.00
O5	0.15			0.12						1.74					2.01
O6						0.54				1.50					2.04
O7				0.07				0.48		1.47					2.02
O8				0.14				0.50		1.43					2.07
O9		0.23									1.59				1.82
O10		0.20									1.56				1.76
O11								0.50			1.46				1.96
O12						0.51					1.40				1.91
O13		0.13	0.13									1.62			1.88
O14			0.08				0.50					1.47			2.05
O15								0.54				1.49			2.03
O16			0.12				0.50					1.47			2.09
O17	0.21												1.63		1.84
O18	0.17												1.53		1.70
O19							0.51						1.41		1.92
O20								0.48					1.37		1.85
O21	0.12			0.13										1.64	1.89
O22							0.50							1.52	2.02
O23				0.13	0.55									1.41	2.09
O24				0.10	0.50									1.37	1.97
O25	0.05				1.81										1.86
O26		0.11			1.81										1.92
O27	0.06					1.87									1.93
O28		0.05				1.85									1.90
O29							1.89								1.89
O30	0.11						1.82								1.93
O31		0.05						1.87							1.92
O32								1.79							1.79
OW1						0.39									0.39
OW2							0.44								0.44
OW3					0.43										0.43
OW4					0.45										0.45
OW5				0.10											0.10
OW6			0.11												0.11
OW7		0.09													0.09
OW8	0.08														0.08
OW9				0.10											0.10
OW10			0.13												0.13
sum	0.94	0.99	0.91	0.89	6.09	6.15	6.16	6.15	5.93	6.15	6.02	6.05	5.94	5.95	

* NH_4^+–O bond valence parameters from Garcia-Rodriguez et al. (2000); U^{+6}–O and S^{+6}–O bond-valence parameters from Gagné and Hawthorne (2015). Hydrogen bond contributions are not included.

Figure 1

Figure 2

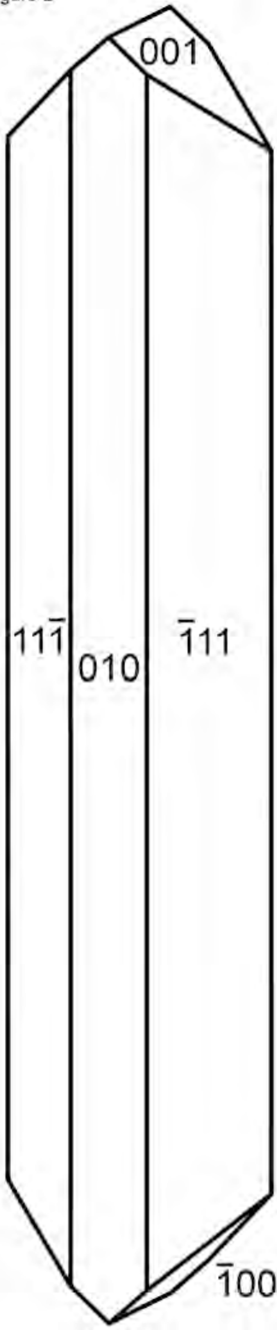

Figure 3

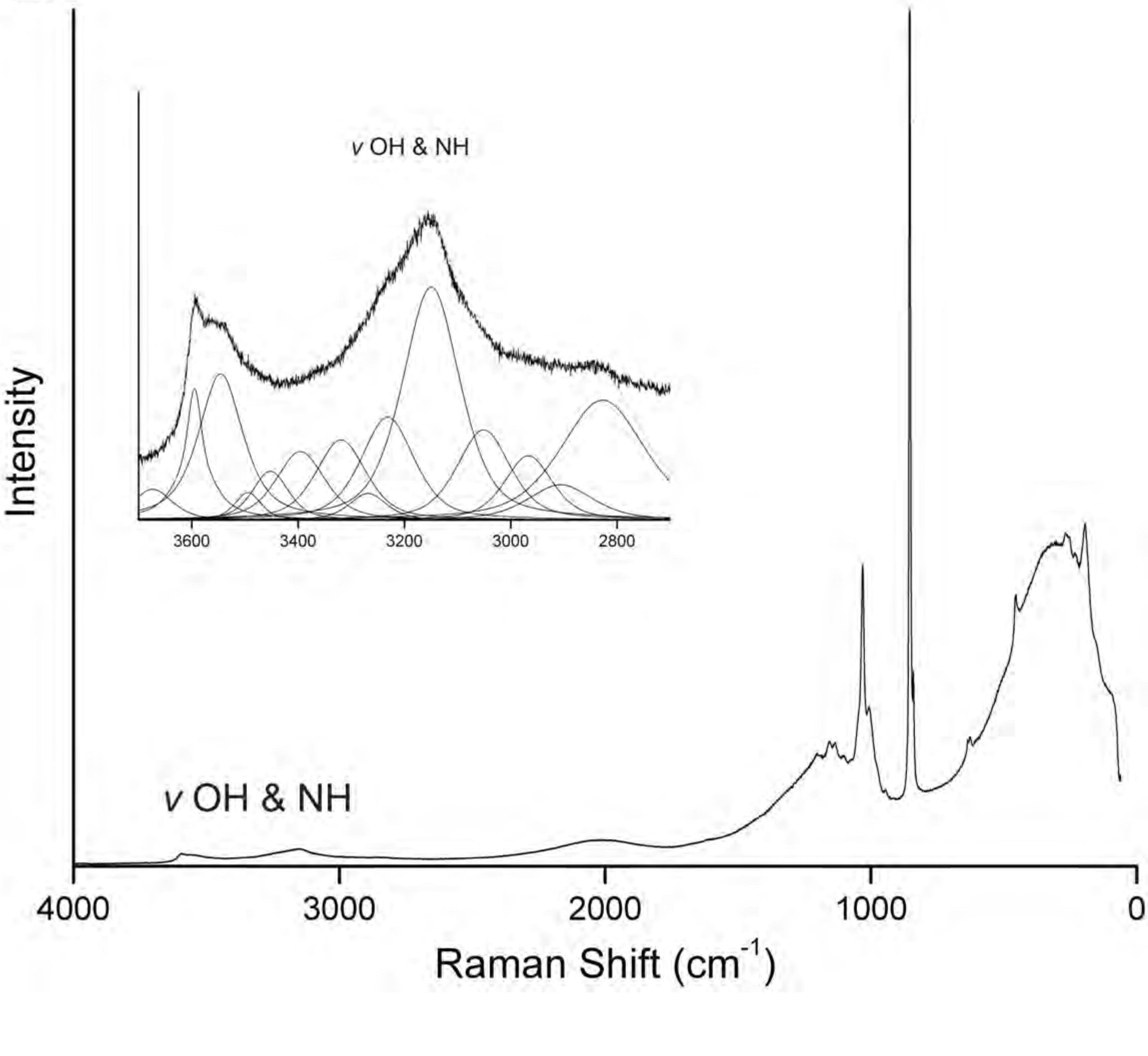

ν OH & NH
3600
3400
3200
3000
2800
Intensity
ν OH & NH
4000
3000
2000
1000
0
Raman Shift (cm-1)

Figure 4

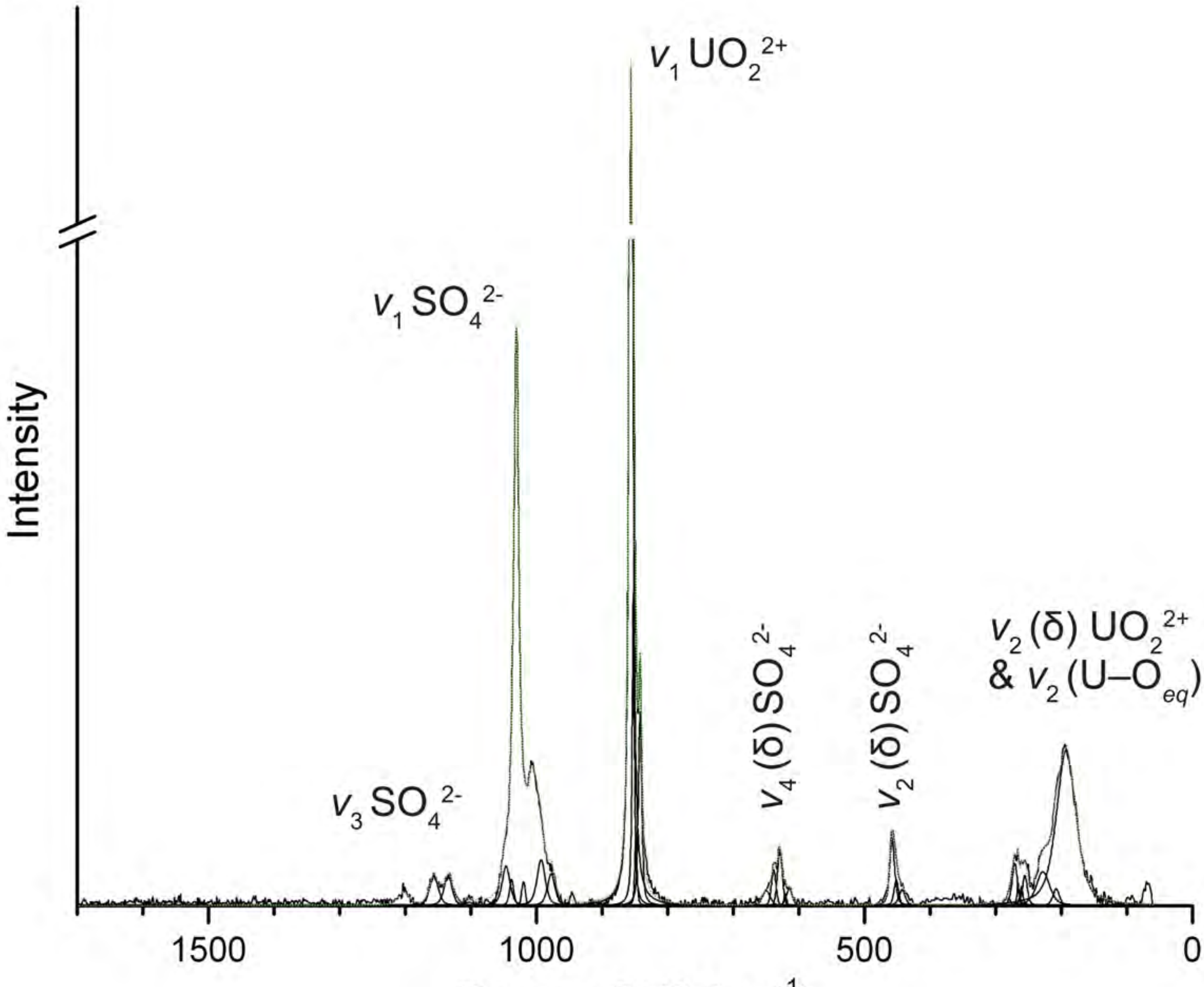

ν_1 UO_2^{2+}
ν_1 SO_4^{2-}
Intensity
ν_3 SO_4^{2-}
ν_4 (δ) SO_4^{2-}
ν_2 (δ) SO_4^{2-}
ν_2 (δ) UO_2^{2+}
& ν_2 (U–O_{eq})
1500
1000
500
0
Raman Shift (cm^{-1})

Figure 5

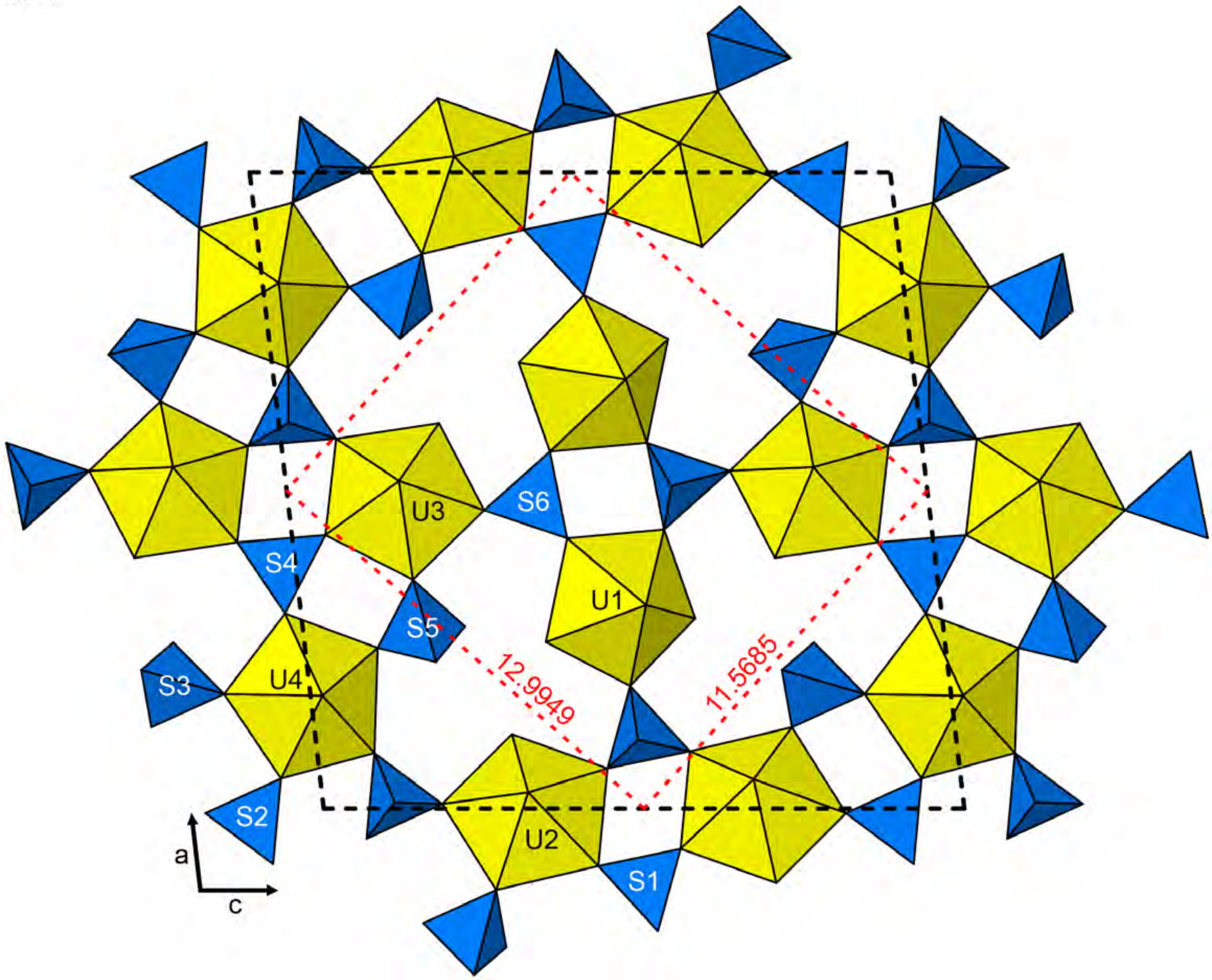

Figure 6

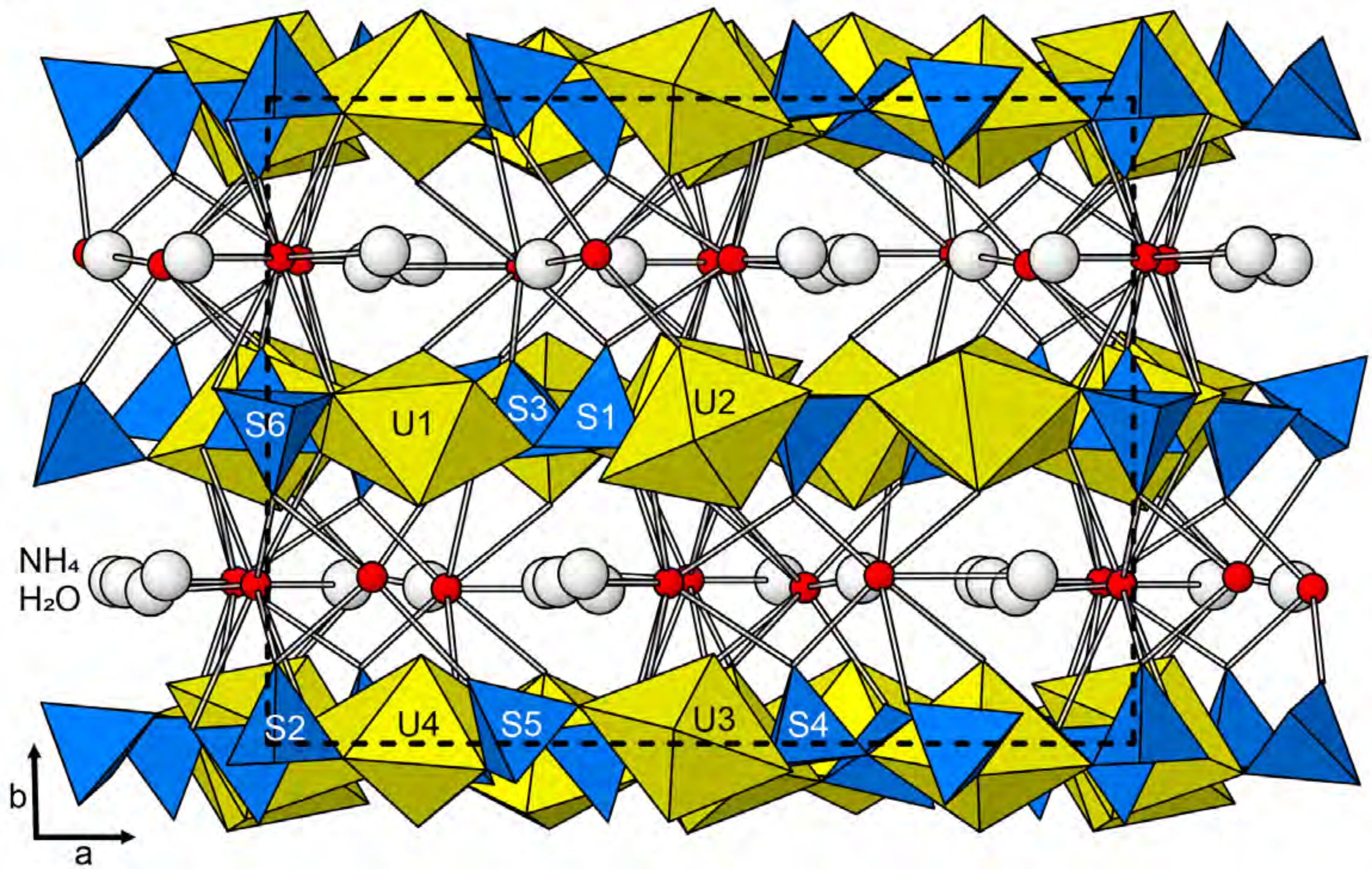

Figure 7